Quantum graphs and the integer quantum Hall effect

N. Goldman and P. Gaspard

Center for Nonlinear Phenomena and Complex Systems, Université Libre de Bruxelles, Code Postal 231, Campus Plaine,
B-1050 Brussels, Belgium

We study the spectral properties of infinite rectangular quantum graphs in the presence of a magnetic field. We study how these properties are affected when three-dimensionality is considered, in particular, the chaological properties. We then establish the quantization of the Hall transverse conductivity for these systems. This quantization is obtained by relating the transverse conductivity to topological invariants. The different integer values of the Hall conductivity are explicitly computed for an anisotropic diffusion system which leads to fractal phase diagrams.

I. INTRODUCTION

Quantum graphs have been the focus of much interest during the last 30 years.[1–3] These models which describe the propagation of a quantum wave within an arbitrary complex object are extremely versatile allowing the study of various interesting quantum phenomena. Quantum graphs appear in various fields such as solid state physics, quantum chemistry, chaology, and wave physics. Basically, quantum graphs describe wave propagation through fine structures. In the field of quantum chemistry, graphs have been used to represent π-electronic orbitals in organic molecules formed with double chemical bonds.[4] In nanotechnology as for future quantum computer devices, they modelize thin conductor circuits that propagate information. They also describe fine superconducting circuits and wave guides leading to acoustic, optic, and electromagnetic applications. Generally speaking, graphs constitute useful models for the description of quantum transport on connected systems.[3]

In the context of quantum chaology, graphs have been the vehicle to confirm important conjectures about chaos signatures. Kottos and Smilansky discovered that periodic-orbit theory exactly applies to quantum graphs and that their spectra may obey the Wigner level spacing statistics under certain conditions.[5] A minimum of three incommensurate bond lengths is required for Wigner level repulsion to already manifest itself.[6] Furthermore, graphs are simple models of quantum scattering and a semiclassical bound has been obtained on their quantum lifetimes.[7] In the classical limit, the scattering is typically stochastic at each vertex of the graph so that the classical dynamics may be chaotic with a positive Kolmogorov-Sinai entropy per unit time on graphs with more than two vertices.[8]

In this paper, we propose to study the integer quantum Hall effect (IQHE) on the basis of quantum graphs. This phenomenon which is manifested by the quantization of the Hall conductance is the object of many works since its discovery by von Klitzing.[9] Thouless *et al.*[10] showed the important link between the Hall conductance and the energy spectra of an independent electron's model, a result which led Osadchy and Avron[11] to draw the phase diagram for Hofstadter's model.[12] This phase diagram is fractal and depicts infinitely many phases, each one characterized by the integer value of the Hall conductance. Such fractal phase diagrams have also been studied in cold atomic systems submitted to artificial gauge fields[13] and in models featuring continuous potentials which exhibit classical chaos.[14,15]

In this context, quantum graphs are interesting because the propagative medium is formed of one-dimensional continuous bonds, in contrast to the fully discrete lattices of the usual tight-binding models. Yet, quantum graphs are simple enough that they can be investigated by analytical developments, as we shall show. It is worth noticing that the band spectra associated to rectangular quantum graphs already exhibit hidden fractal structures in the absence of an external field.[16]

We first study the energy spectra for infinite rectangular graphs perturbed by a strong magnetic field. We obtain the spectral properties of two-dimensional (2D) and three-dimensional (3D) systems. This allows us to compare these systems from the viewpoint of chaology. We show that the eigenvalue equation of quantum graphs can be mapped onto the generalized Harper equation in the case of 2D rectangular lattices. We then compute the transverse conductivity of the 2D system with Kubo's formula which describes the linear response of this system to an external electric field, and obtain the quantization law through topological arguments. We then show the link between the Hall conductivity and the energy spectra by computing this quantity for Fermi energies located inside the many gaps of the spectra. We conclude this work with the presentation of a fractal phase diagram which describes the IQHE on 2D as well as 3D quantum graphs.

The paper is organized as follows. The spectral properties of 2D and 3D quantum graphs are, respectively, presented in Secs. II and III. The Hall conductivity on quantum graphs is studied in Sec. IV. The conclusions are drawn in Sec. V.

II. TWO-DIMENSIONAL QUANTUM GRAPHS

A. Eigenvalue equation

A quantum graph is a set of vertices connected by unidimensional bonds on which a quantum wave propagates. Each bond of a rectangular lattice is characterized by a vertex coordinate (n,m) and by a direction $b=1,2$, and will be labeled (n,m,b). Schrödinger's equation is satisfied on each bond,

$$\left(-i\frac{d}{dr_b} - A^{(n,m,b)}\right)^2 \psi^{(n,m,b)}(r_b) = k^2 \psi^{(n,m,b)}(r_b), \qquad (1)$$

where $A^{(n,m,b)}$ is the potential vector component along the bond b, $k=\sqrt{2ME}/\hbar$ is the wave number, and M and E are, respectively, the mass and the energy of the particle. In the following, we use units where $M=1$ and $\hbar=1$, except otherwise stated. We consider an infinite graph forming a rectangular lattice submitted to a magnetic field $\boldsymbol{B}=\boldsymbol{\nabla}\times\boldsymbol{A}$ and we work in the Lorentz gauge $\boldsymbol{A}=(0,Bx,0)$, which maintains a discrete translational invariance along the y direction. We suppose that the different bonds are directed along the x (y) axis with constant length l_x (l_y). The wave function $\psi^{(n,m,1)}(x)$ $[\psi^{(n,m,2)}(y)]$ is defined between vertex (n,m) and $(n+1,m)$ $[(n,m)$ and $(n,m+1)]$. Accordingly, we have that $x\in[0;l_x]$ and $y\in[0;l_y]$.

The solutions of Schrödinger's equation (1) are written as

$$\psi^{(n,m,1)}(x) = C_1^{(n,m,1)}e^{ikx} + C_2^{(n,m,1)}e^{-ikx},$$

$$\psi^{(n,m,2)}(y) = C_1^{(n,m,2)}e^{iky+iBnl_xy} + C_2^{(n,m,2)}e^{-iky+iBnl_xy}. \qquad (2)$$

We consider an anisotropic scattering model which results from the modification of the usual boundary conditions imposed at each vertex.[5,16] We introduce two parameters s and r in these conditions,

$$\psi^{(n,m,1)}(x=0) = \psi^{(n-1,m,1)}(x=l_x) = s\psi^{(n,m,2)}(y=0)$$
$$= s\psi^{(n,m-1,2)}(y=l_y), \qquad (3)$$

$$r\left[\frac{d\psi^{(n,m,1)}}{dx}(x=0) - \frac{d\psi^{(n-1,m,1)}}{dx}(x=l_x)\right] + \frac{d\psi^{(n,m,2)}}{dy}(y=0)$$
$$- \frac{d\psi^{(n,m-1,2)}}{dy}(y=l_y) - iBnl_x[\psi^{(n,m,2)}(y=0)$$
$$- \psi^{(n,m-1,2)}(y=l_y)] = 0, \qquad (4)$$

where the particular case $r=s=1$ corresponds to an isotropic graph. One has to impose the unitarity of the scattering matrix $\hat{S}$. This matrix which plays an important role in the theory of quantum graphs links the in-components χ^{in} to the out-components χ^{out} at each vertex. These components are written as follows for our model:

$$\chi^{\text{out}} = \begin{pmatrix} C_1^{(n,m,1)} \\ C_1^{(n,m,2)} \\ C_2^{(n-1,m,1)}e^{-ikl_x} \\ C_2^{(n,m-1,2)}e^{-ikl_y+iBnl_xl_y} \end{pmatrix},$$

$$\chi^{\text{in}} = \begin{pmatrix} C_2^{(n,m,1)} \\ C_2^{(n,m,2)} \\ C_1^{(n-1,m,1)}e^{ikl_x} \\ C_1^{(n,m-1,2)}e^{ikl_y+iBnl_xl_y} \end{pmatrix}, \qquad (5)$$

where $C_{1,2}^{(n,m,b)}$ are the coefficients of the functions $\psi^{(n,m,b)}$ as defined in Eqs. (2). The scattering matrix is then given by

$$\hat{S} = \frac{1}{rs+1}\begin{pmatrix} -1 & s & rs & s \\ r & -rs & r & 1 \\ rs & s & -1 & s \\ r & 1 & r & -rs \end{pmatrix} \qquad (6)$$

and the unitarity condition $\hat{S}^\dagger\hat{S}=\hat{S}\hat{S}^\dagger=\hat{I}$ sets $r=s$. The unitarity condition guarantees the conservation of probability at each vertex. This latter is expressed as

$$j^{(n-1,m,1)} + j^{(n,m-1,2)} = j^{(n,m,1)} + j^{(n,m,2)} \qquad (7)$$

with the probability current densities:

$$j^{(n,m,b)} = \frac{1}{2i}\left(\psi^{(n,m,b)*}\frac{d\psi^{(n,m,b)}}{dr_b} - \frac{d\psi^{(n,m,b)*}}{dr_b}\psi^{(n,m,b)}\right)$$
$$- A^{(n,m,b)}|\psi^{(n,m,b)}|^2. \qquad (8)$$

One can then write the solutions (2) in the following form:

$$\psi^{(n,m,1)}(x) = f_{n,m}\frac{\sin k(l_x-x)}{\sin kl_x} + f_{n+1,m}\frac{\sin kx}{\sin kl_x},$$

$$\psi^{(n,m,2)}(y) = \frac{1}{r}f_{n,m}e^{iBnl_xy}\frac{\sin k(l_y-y)}{\sin kl_y}$$
$$+ \frac{1}{r}f_{n,m+1}e^{iBnl_x(y-l_y)}\frac{\sin ky}{\sin kl_y}, \qquad (9)$$

where the coefficients $f_{n,m}$ are defined by

$$f_{n,m} = \psi^{(n,m,1)}(x=0) = r\psi^{(n,m,2)}(y=0)$$
$$= C_1^{(n,m,1)} + C_2^{(n,m,1)} = r(C_1^{(n,m,2)} + C_2^{(n,m,2)}),$$

$$f_{n+1,m} = \psi^{(n,m,1)}(x=l_x) = C_1^{(n,m,1)}e^{ikl_x} + C_2^{(n,m,1)}e^{-ikl_x},$$

$$f_{n,m+1} = r\psi^{(n,m,2)}(y=l_y)$$
$$= r(C_1^{(n,m,2)}e^{ikl_y+i2\pi\Phi n} + C_2^{(n,m,2)}e^{-ikl_y+i2\pi\Phi n}). \qquad (10)$$

Here, $\Phi=Bl_xl_y/(2\pi)$ is the magnetic flux through a unit cell and the condition (3) has been applied.

The system being invariant under discrete translations along the y axis, we are led to consider new wave functions $u^{(n,b)}$ defined in terms of the solutions $\psi^{(n,m,b)}$ of Eq. (1) according to

$$u^{(n,1)}(x) \equiv \psi^{(n,m,1)}(x)e^{-ik_xnl_x-ik_yml_y}, \qquad (11)$$

$$u^{(n,2)}(y) \equiv \psi^{(n,m,2)}(y)e^{-ik_xnl_x-ik_yml_y}. \qquad (12)$$

Similarly, the coefficients g_n are defined as

$$g_n \equiv f_{n,m}e^{-ik_xnl_x-ik_yml_y}. \qquad (13)$$

According to Eqs. (9), the new wave functions $u^{(n,b)}$ are written in terms of new coefficients (13) as

$$u^{(n,1)}(x) = g_n\frac{\sin k(l_x-x)}{\sin kl_x} + g_{n+1}\frac{\sin kx}{\sin kl_x}e^{ik_xl_x}, \qquad (14)$$

$$u^{(n,2)}(y) = \frac{1}{r}g_n\left[e^{iBnl_xy}\frac{\sin k(l_y - y)}{\sin kl_y} + e^{iBnl_x(y-l_y)}\frac{\sin ky}{\sin kl_y}e^{ik_yl_y}\right].$$

(15)

The probability conservation (4) implies

$$e^{ik_xl_x}g_{n+1} + e^{-ik_xl_x}g_{n-1} + \frac{2}{r^2}\frac{\sin kl_x}{\sin kl_y}\cos(2\pi\Phi n - k_yl_y)g_n$$

$$= 2\left(\cos kl_x + \frac{\cos kl_y}{r^2}\frac{\sin kl_x}{\sin kl_y}\right)g_n.$$

(16)

If we set

$$\Lambda = \frac{1}{r^2}\frac{\sin kl_x}{\sin kl_y},$$

(17)

$$\mathcal{E} = 2\left(\cos kl_x + \frac{\cos kl_y}{r^2}\frac{\sin kl_x}{\sin kl_y}\right)$$

(18)

one finds the generalized Harper equation

$$e^{ik_xl_x}g_{n+1} + e^{-ik_xl_x}g_{n-1} + 2\Lambda\cos(2\pi\Phi n - k_yl_y)g_n = \mathcal{E}g_n,$$

(19)

which reduces to Harper's equation for Hofstadter's model when $l_x = l_y$ and $r = 1$. This shows that the problem of the quantum graph can be mapped onto a similar problem for the anisotropic tight-binding Hamiltonian with the transfer coefficients t_a and t_b.[18] The correspondence is established with the anisotropy ratio $\Lambda = t_b/t_a$. However, an important difference is that the parameter Λ and the energy $\mathcal{E}$ are independent in the tight-binding model, albeit they both depend on the wave number $k = \sqrt{2E}$ in the quantum graph. In this regard, the eigenvalue problem is more complicated in quantum graphs.

We notice that we would have obtained the dual generalized Harper equation

$$e^{ik_yl_y}h_{m+1} + e^{-ik_yl_y}h_{m-1} + \frac{2}{\Lambda}\cos(2\pi\Phi m + k_xl_x)h_m = \frac{\mathcal{E}}{\Lambda}h_m$$

(20)

if we had used another gauge with the vector potential $A' = (-By, 0, 0)$. In principle, the eigenvalue equations (19) and (20) should lead to the same energy spectrum since they correspond to the same magnetic field $B = \nabla\times A' = \nabla\times A$. Indeed, Eq. (20) is derived from Eq. (19) thanks to the duality transformation[22]

$$h_m \equiv \sum_{n=-\infty}^{+\infty} g_n e^{-i2\pi\Phi mn}.$$

(21)

Our aim is to obtain the spectra in the plane of the magnetic flux Φ versus the wave number $k = \sqrt{2E}$. This latter is directly related to the energy $E = k^2/2$ and has the advantage to be well-adapted to quantum graphs since the spectra tend to distribute themselves uniformly along the wave number k axis, which is not the case along the energy axis. The method to obtain the spectra is to consider the rational values of the magnetic flux $\Phi = p/q$, with $p, q \in \mathbb{Z}$. The rational numbers

are dense in the real numbers so that we may hope to display the structure of the spectrum by plotting the spectra for all the rational numbers $\Phi = p/q$ up to a large enough integer q.

If the magnetic flux is rational $\Phi = p/q$, we may assume that the functions $u^{(n,b)}$ satisfy the periodic boundary conditions

$$u^{(n+q,1)}(x) = u^{(n,1)}(x),$$

$$u^{(n+q,2)}(y) = u^{(n,2)}(y)e^{i2\pi py/l_y}.$$

(22)

In this case, the Bloch parameters take their values in the ranges $k_x \in \left[-\frac{\pi}{ql_x}, \frac{\pi}{ql_x}\right]$ and $k_y \in \left[-\frac{\pi}{l_y}, \frac{\pi}{l_y}\right]$ which delimit the first Brillouin zone.

As a consequence of Eqs. (11), (12), and (22), the coefficients (13) satisfy the periodic condition

$$g_{n+q} = g_n,$$

(23)

and the eigenvalue equation (19) can be solved by requiring that the corresponding characteristic $q \times q$ determinant vanishes.

B. Quantum graphs without magnetic field

If the magnetic flux vanishes $\Phi = 0$, the eigenvalue equation (16) can be solved by taking $g_{n+1} = g_n$. The eigenvalues are thus given by the zeros of the following function of the wave number k:

$$f(k) = r^2(\cos kl_x - \cos k_xl_x)\sin kl_y + (\cos kl_y - \cos k_yl_y)\sin kl_x$$

$$= 0.$$

(24)

For fixed values of Bloch's parameters k_x and k_y, the spectrum is discrete. A continuous band spectrum is obtained by varying Bloch's parameters in the first Brillouin zone delimited by $k_x \in \left[-\frac{\pi}{l_x}, \frac{\pi}{l_x}\right]$ and $k_y \in \left[-\frac{\pi}{l_y}, \frac{\pi}{l_y}\right]$. An example of the band spectrum is depicted in Fig. 1.

For fixed values of the Bloch parameters, the spectrum is discrete as aforementioned. In this case, we can study the statistics of the level spacings:

$$S = \frac{k_{i+1} - k_i}{\langle k_{i+1} - k_i\rangle},$$

(25)

where k_i with $i \in \mathbb{N}$ are the roots of Eq. (24): $f(k_i) = 0$. We observe in Fig. 2 that the level spacing distribution is empty around zero spacing for $k_xl_x = 1$ and $k_yl_y = 0.7$. This gap is due to the fact that there are only two incommensurate lengths l_x and l_y in the 2D graph. As a consequence, it is known that the spacing distribution should generically present such a gap.[6]

In the classical limit, point particles move with the velocity v on the one-dimensional bonds and are scattered stochastically at each vertex.[8] In the case where $r = 1$, the probability to be scattered in one of the four directions of the lattice are equal to $1/4$. Accordingly, the particle undergoes a diffusive random walk on the lattice, the properties of which can be calculated with the methods of Ref. 8. The diffusion coefficients take the values $D_x = \frac{vl_x^2}{2(l_x+l_y)}$ and $D_y = \frac{vl_y^2}{2(l_x+l_y)}$. The Kolmogorov-Sinai entropy per unit time is equal to h_{KS}
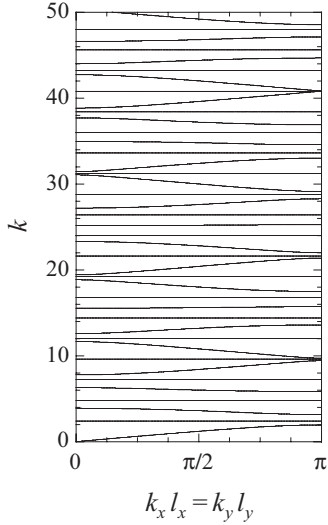
FIG. 1. Band spectrum of the 2D graph without magnetic field $\Phi=0$. The bond lengths are $l_x=1$ and $l_y=(1+\sqrt{5})/2$. The bands are depicted in the plane of the wave number $k=\sqrt{2E}$ versus the Bloch parameters $k_x l_x = k_y l_y$.

$=\frac{v\ln 4}{l_x+l_y}$ and its positivity shows that the classical motion is chaotic.

C. Quantum graphs with magnetic field

We solve numerically the generalized Harper equation in order to obtain the energy spectrum as a function of the magnetic flux. Several spectra are shown in Figs. 3(a)–3(d) in terms of the wave number $k=\sqrt{2E}$ for the cases $l_x=1$, 1.5, 2, and 2.5 with $l_y=1$ and $r=1$.

In the case $l_x=l_y=1$ and $r=1$, the lattice has the square symmetry and the spectrum in Fig. 3(a) resembles the Hofstadter butterfly.[12] We can show that it is identical to the Hofstadter butterfly up to a deformation. Indeed, Eqs. (17) and (18) give $\Lambda=1$ and $\mathcal{E}=4\cos k$ in this case. Accordingly,
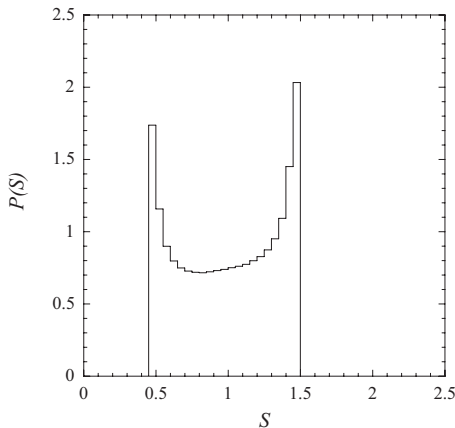

FIG. 2. The level spacing probability density $P(S)$ for the 2D graph without magnetic field $\Phi=0$ at the values $k_x l_x=1$ and $k_y l_y=0.7$ of Bloch parameters. The bond lengths are $l_x=1$ and $l_y=(1+\sqrt{5})/2$. We observe the expected gap around zero spacing.

Eq. (19) reduces to Harper's equation which leads to the Hofstadter butterfly represented in the plane of the magnetic flux Φ versus the energy $\mathcal{E}$. Figure 3(a) depicts the butterfly versus the wave number $k=\arccos(\mathcal{E}/4)$. The butterfly is thus only deformed by this change of variable.

However, the anisotropy enhanced by the difference $l_x \neq l_y$ closes many gaps [dark zones in Figs. 3(b)–3(d)], which reminds us of a similar phenomenon observed in the anisotropic Hofstadter model.[18] The spectrum of the latter model is described by the Harper equation (19) and is darkened when the anisotropy ratio $\Lambda=\frac{t_b}{t_a}$ differs from unity. We have a similar phenomenon in the spectrum of quantum graphs although it is complicated by the common dependence of Λ and $\mathcal{E}$ on the wave number k. We observe that the dark zones appear away from the values k_s of the wave number for which the anisotropy coefficient is close to unity: $\Lambda = \left| \frac{\sin k_s l_x}{r^2 \sin k_s l_y} \right| \simeq 1$. The reasons are that the generalized Harper equations (19) and (20) are known to admit extended eigenstates if Λ is different from unity,[22] and that continuous spectra are typically associated with extended eigenstates. In contrast, the spectrum displays fractal structures reminiscent of the Hofstadter butterfly around the special values k_s where the anisotropy ratio approaches unity.

In the case $l_x=1.5$ depicted in Fig. 3(b), the anisotropy ratio is unity if $|\sin k_s|=|\sin(3k_s/2)|$. This condition is satisfied at $k_s=\frac{2\pi}{5},\frac{4\pi}{5},\frac{6\pi}{5},\frac{8\pi}{5},\ldots$. We clearly see in Fig. 3(b) that the spectrum displays the fractal structures of the Hofstadter butterfly around these values, while it darkens away. Similarly, we see in the case $l_x=2$ depicted in Fig. 3(c) that the spectrum looks locally as the Hofstadter butterfly around the special values $k_s=\frac{\pi}{3},\frac{2\pi}{3},\frac{4\pi}{3},\frac{5\pi}{3},\ldots$ where $\Lambda=1$.

In the case $l_x=2.5$ depicted in Fig. 3(d), this also happens around the special values $k_s=0.898,1.795,2.094,2.693,3.590,4.189,4.488,5.386,\ldots$ where $\Lambda=1$. Here, the situation is more subtle because, for instance, the values $k_s=1.795$ and 2.094 are very close to each other and the anisotropy ratio remains close to unity between these values. This explains that the spectrum looks as a Hofstadter butterfly only once in this interval and similarly for $4.189 < k_s < 4.488$.

We notice that the spectra are periodic in the wave number if the two lengths l_x and l_y are commensurate. They form nonperiodic structures as the wave number increases if the lengths are incommensurate. We finally note that for $l_x=l_y=n$, where n is an integer, the spectrum represents exactly n Hofstadter butterflies for $k \in [0,\pi]$. In the anisotropic situations depicted in Fig. 3(c) in which $l_x=n$ and $l_y=1$, we find exactly n butterflylike structures for $k \in [0,\pi]$.

III. THREE-DIMENSIONAL QUANTUM GRAPHS

A. Eigenvalue equation

The insertion of a third dimension in quantum graphs submitted to magnetic fields is expected to yield drastic changes in the spectral properties of these systems. Recent works have been investigating the effects due to three-dimensionality in the Hofstadter model.[19–21] These studies led to the conclusion that Hofstadter butterflylike fractal pat-
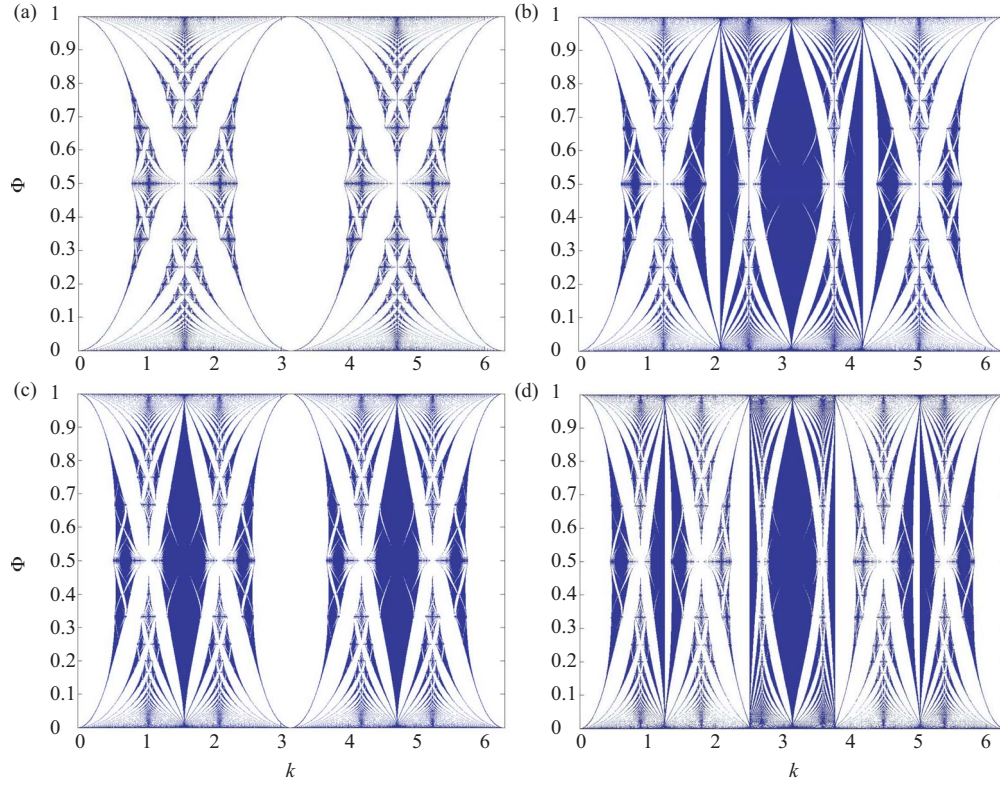
FIG. 3. (Color online) Spectra of the quantum graphs for the cases: (a) $l_x=1$, (b) $l_x=1.5$, (c) $l_x=2$, and (d) $l_x=2.5$ with $l_y=1$ and $r=1$. The wave number $k=\sqrt{2E}$ is along the horizontal axis and the magnetic flux Φ along the vertical axis.

terns still exist in 3D space systems under certain conditions.

We here show that fractal patterns also persist in 3D quantum graphs. Each bond of the 3D lattice is characterized by a vertex coordinate (n,m,l) and by a direction $b=1,2,3$, and will be labeled (n,m,l,b). We suppose that the magnetic field is still oriented along the z axis and that we work with the Lorentz gauge where $A=(0,Bx,0)$, so that the wave function along the bond $(n,m,l,3)$ is a solution of the Schrödinger equation

$$\left(-i\frac{d}{dz}\right)^2\psi^{(n,m,l,3)}(z)=k^2\psi^{(n,m,l,3)}(z). \quad (26)$$

We can then treat this system using the method described in Sec. II. We impose boundary conditions similar to the 2D case with

$$\frac{d\psi^{(n,m,l,1)}}{dx}(x=0)-\frac{d\psi^{(n-1,m,l,1)}}{dx}(x=l_x)+\frac{d\psi^{(n,m,l,2)}}{dy}(y=0)$$

$$-\frac{d\psi^{(n,m-1,l,2)}}{dy}(y=l_y)-iBnl_x[\psi^{(n,m,l,2)}(y=0)$$

$$-\psi^{(n,m-1,l,2)}(y=l_y)]+\gamma\left[\frac{d\psi^{(n,m,l,3)}}{dz}(z=0)\right.$$

$$\left.-\frac{d\psi^{(n,m,l-1,3)}}{dz}(z=l_z)\right]=0, \quad (27)$$

where the parameter $\gamma\in[0,1]$ maps the 2D system ($\gamma=0$) to the 3D isotropic system ($\gamma=1$).

The wave function is explicitly written as

$$\psi^{(n,m,l,3)}(z)=f_{n,m,l}\frac{\sin k(l_z-z)}{\sin kl_z}+f_{n,m,l+1}\frac{\sin kz}{\sin kl_z}. \quad (28)$$

Setting

$$g_n\equiv f_{n,m,l}e^{-ik_xnl_x-ik_yml_y-ik_zll_z} \quad (29)$$

with $k_x\in\left[-\frac{\pi}{ql_x},\frac{\pi}{ql_x}\right]$, $k_y\in\left[-\frac{\pi}{l_y},\frac{\pi}{l_y}\right]$, and $k_z\in\left[-\frac{\pi}{l_z},\frac{\pi}{l_z}\right]$, one finds the generalized 3D Harper equation

$$e^{ik_xl_x}g_{n+1}+e^{-ik_xl_x}g_{n-1}+[2\Lambda\cos(2\pi\Phi n-k_yl_y)$$

$$+2\tilde{\Lambda}\cos k_zl_z]g_n=\mathcal{E}g_n \quad (30)$$

with the coefficients

$$\Lambda=\frac{\sin kl_x}{\sin kl_y}, \quad (31)$$

$$\tilde{\Lambda}=\gamma^2\frac{\sin kl_x}{\sin kl_z}, \quad (32)$$

$$\mathcal{E}=2(\cotg kl_x+\cotg kl_y+\gamma^2\cotg kl_z)\sin kl_x. \quad (33)$$

As in the 2D system, these coefficients all depend on the wave number k.

B. Quantum graphs without magnetic field

If the magnetic flux vanishes $\Phi=0$, we may assume that the solution is periodic with $g_{n+1}=g_n$, in which case the ei-
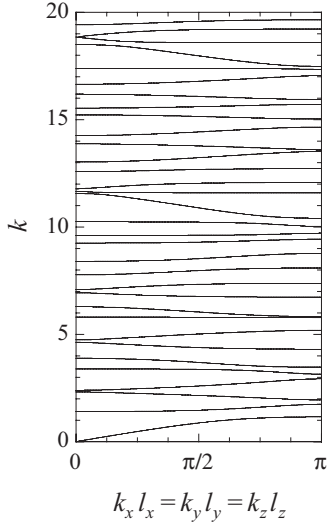
FIG. 4. Band spectrum of the 3D graph without magnetic field $\Phi=0$. The bond lengths are $l_x=1$, $l_y=(1+\sqrt{5})/2$, and $l_z=\exp(1)$. The bands are depicted in the plane of the wave number $k=\sqrt{2E}$ versus the Bloch parameters $k_x l_x = k_y l_y = k_z l_z$.

genvalue equation (30) with the coefficients (31)–(33) becomes

$$
\begin{aligned}
f(k) = {}& (\cos kl_x - \cos k_x l_x)\sin kl_y \sin kl_z \\
& + (\cos kl_y - \cos k_y l_y)\sin kl_x \sin kl_z \\
& + \gamma^2(\cos kl_z - \cos k_z l_z)\sin kl_x \sin kl_y = 0. \quad (34)
\end{aligned}
$$

Because of its spatial periodicity, the system has continuous band spectra, an example of which is depicted in Fig. 4. Contrary to the 2D system, Wigner repulsion manifests itself in the level spacing statistics. The Wigner repulsion has for consequence that a typical level spacing probability density behaves as $P(S) \sim S$ for $S \to 0$, as observed in Fig. 5. Consequently, there is no gap at small level spacings contrary to what happens in Fig. 2 for the 2D case. The reason is that the 3D lattices typically have three incommensurate lengths, which is the minimum number for Wigner repulsion to manifest itself.[6]
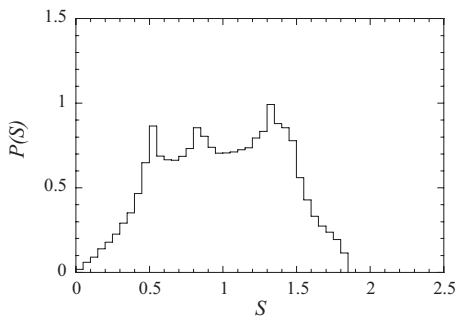

FIG. 5. The level spacing probability density $P(S)$ for the 3D graph without magnetic field $\Phi=0$ at the values $k_x l_x=1.5$, $k_y l_y=1$, and $k_z l_z=0.7$ of Bloch parameters. The bond lengths are $l_x=1$, $l_y=(1+\sqrt{5})/2$, and $l_z=\exp(1)$. We observe the behavior characteristic of Wigner repulsion: $P(S) \sim S$ for $S \to 0$.
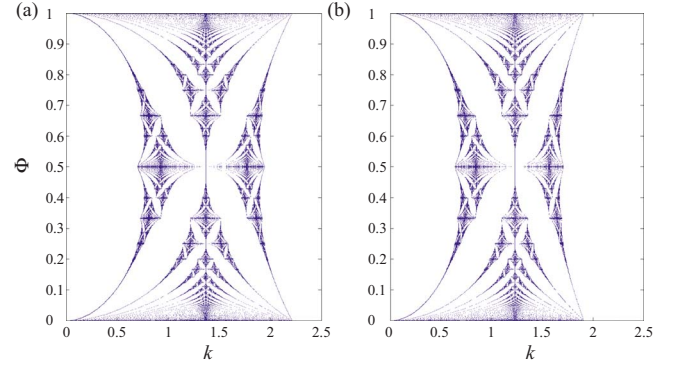

FIG. 6. (Color online) Spectra of the quantum graphs for (a) $\gamma=0.5$ and (b) $\gamma=1$, with $l_x=l_y=l_z=1$ and $k_z=0$. The wave number $k=\sqrt{2E}$ is along the horizontal axis and the magnetic flux Φ along the vertical axis.

C. Quantum graphs with magnetic field

We solved the generalized 3D Harper equation (30) with $\Phi \neq 0$ in order to find the spectrum associated to the system for different values of γ. As shown in Fig. 6, the butterfly seems to lose its initial symmetric shape as γ differs from zero, and eventually forms a new fractal structure for $\gamma=1$. It is worth noticing that the many gaps which compose the Hofstadter butterfly are conserved as one maps the 2D system to the 3D system. Figure 6 depicts the spectra corresponding to a single value of the Bloch parameter k_z, which corresponds to the situation of a very flattened 3D system. As the graph thickens, k_z takes more values between $-\pi/l_z$ and π/l_z and the spectrum appears as the superposition of several deformed butterflies. As the three-dimensionality becomes important, gaps close and the spectrum darkens as shown in Fig. 7.
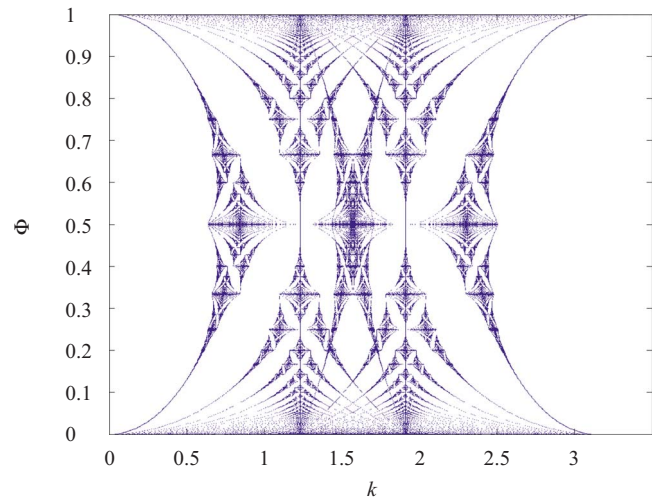

FIG. 7. (Color online) Spectra of the quantum graphs for $\gamma=1$, with $l_x=l_y=l_z=1$ and $k_z=n\pi$, $n \in \mathbb{Z}$. The wave number $k=\sqrt{2E}$ is along the horizontal axis and the magnetic flux Φ along the vertical axis.

IV. QUANTUM HALL EFFECT ON QUANTUM GRAPHS

A. Kubo formula on quantum graphs

In order to study the integer quantum Hall effect, we consider independent Fermions on a 2D quantum graph and evaluate the antisymmetric component $\sigma_{xy} = -\sigma_{yx}$ of the conductivity tensor with Kubo's formula for zero temperature. The latter relates σ_{xy} to the current intensity $\hat{\mathbf{J}} = (\hat{J}_x, \hat{J}_y)$ and can be written in the following way:

$$\sigma_{xy} = \frac{1}{iV} \sum_{\mathbf{N}} \frac{\langle \mathbf{N}|\hat{J}_x|0\rangle\langle 0|\hat{J}_y|\mathbf{N}\rangle - (x \leftrightarrow y)}{(E_0 - E_{\mathbf{N}})^2}, \qquad (35)$$

where $|\mathbf{N}\rangle$ denotes the eigenstates of the many-particle Hamiltonian $\hat{\mathcal{H}}$ of eigenvalue $E_{\mathbf{N}}$, $|0\rangle$ is the ground state, and $V = \Sigma_{(n,m,b)} l_b$ is the system "volume" given by the total lengths of the bonds in a unit cell of the periodic lattice. l_b denotes the length of the bond b.

We define the current density which circulates along the bond (n, m, b) in the direction x by

$$\hat{j}_x^{(n,m,b)} = \frac{1}{2i}\left(\hat{\Psi}^{(n,m,b)\dagger}\frac{d\hat{\Psi}^{(n,m,b)}}{dx} - \frac{d\hat{\Psi}^{(n,m,b)\dagger}}{dx}\hat{\Psi}^{(n,m,b)} \right)$$
$$- A_x^{(n,m,b)}\hat{\Psi}^{(n,m,b)\dagger}\hat{\Psi}^{(n,m,b)}, \qquad (36)$$

where $A_x^{(n,m,b)}$ is the x component of the potential vector along the bond (n, m, b) and $\hat{\Psi}^{(n,m,b)}$ is the field operator defined on the bond. In the second quantization formalism, the field operator and the adjoint field operator are, respectively, given by

$$\hat{\Psi}^{(n,m,b)} = \sum_{\nu} \psi_\nu^{(n,m,b)}\hat{a}_\nu, \qquad (37)$$

$$\hat{\Psi}^{(n,m,b)\dagger} = \sum_{\nu'} \psi_{\nu'}^{(n,m,b)*}\hat{a}_{\nu'}^\dagger, \qquad (38)$$

where $\hat{a}_\nu$ and $\hat{a}_\nu^\dagger$ are the annihilation and creation operators satisfying the anticommutation relation: $\hat{a}_\nu\hat{a}_{\nu'}^\dagger + \hat{a}_{\nu'}^\dagger\hat{a}_\nu = \delta_{\nu\nu'}$. If the system is in the Fock state $|\mathbf{N}\rangle = |N_1 N_2 N_3 \cdots N_\nu \cdots\rangle$ with $N_\nu = 0$ or 1 Fermion on each single-particle wave function ψ_ν, the total energy of the system takes the value

$$E_{\mathbf{N}} = \sum_\nu N_\nu \epsilon_\nu, \qquad (39)$$

where ϵ_ν is the energy corresponding to the single-particle wave function ψ_ν and N_ν is the corresponding occupation number ($N_\nu = 0, 1$).

The current intensity which circulates in a unit cell of the lattice is defined by

$$\hat{J}_x = \sum_{(n,m,b)} \int_0^{l_b} \hat{j}_x^{(n,m,b)} dr_b, \qquad (40)$$

where the sum over (n, m, b) extends over all the bonds of the unit cell. Substituting the expression (36) of the current density and using Eqs. (37) and (38), we find that the current intensity is given by

$$\hat{J}_x = \sum_{(n,m,b)} \sum_{\nu,\nu'} \int_0^{l_b} dr_b \left[\frac{1}{2i}\left(\psi_{\nu'}^{(n,m,b)*}\frac{d\psi_\nu^{(n,m,b)}}{dx} \right.\right.$$
$$\left.\left. - \frac{d\psi_{\nu'}^{(n,m,b)*}}{dx}\psi_\nu^{(n,m,b)} \right) - A_x^{(n,m,b)}\psi_{\nu'}^{(n,m,b)*}\psi_\nu^{(n,m,b)} \right]\hat{a}_{\nu'}^\dagger\hat{a}_\nu$$

$$\qquad (41)$$

$$\equiv \sum_{\nu,\nu'} \langle \nu'|\hat{v}_x|\nu\rangle\hat{a}_{\nu'}^\dagger\hat{a}_\nu. \qquad (42)$$

The quantities $\langle \nu'|\hat{v}_x|\nu\rangle$ which are here introduced are the matrix elements of the particle velocity in the single-particle wave functions ψ_ν. The scalar product in the space of the single-particle wave functions on the graph is defined by

$$\langle \phi|\psi\rangle = \sum_{(n,m,b)} \int_0^{l_b} \phi^{(n,m,b)*}\psi^{(n,m,b)} dr_b, \qquad (43)$$

where the sum $\Sigma_{(n,m,b)}$ accounts for the contribution of all the bonds in the unit cell.

Since the operator $\hat{J}_x$ contains one annihilation and one creation operator, the matrix element $\langle \mathbf{N}|\hat{J}_x|0\rangle$ is nonvanishing only for Fock states

$$|\mathbf{N}\rangle = |111\cdots 111\underbrace{0}_{\alpha}111\cdots 111\underset{\epsilon_{\mathrm{F}}}{\uparrow}000\cdots 000\underbrace{1}_{\beta}000\cdots\rangle \qquad (44)$$

with one hole and one particle. ϵ_{F} denotes the Fermi energy. Indeed, applying an annihilation operator followed by a creation operator on the ground state gives such a state up to a phase:

$$\hat{a}_\beta^\dagger\hat{a}_\alpha|111\cdots 111\underset{\epsilon_{\mathrm{F}}}{\uparrow}000\cdots 000\cdots\rangle$$
$$= (-1)^{\alpha+N_{\mathrm{F}}}|111\cdots 111\underbrace{0}_{\alpha}111\cdots 111\underset{\epsilon_{\mathrm{F}}}{\uparrow}000$$
$$\cdots 000\underbrace{1}_{\beta}000\cdots\rangle, \qquad (45)$$

where N_{F} is the total number of Fermions and α the integer labeling the corresponding single-particle state. Therefore the matrix element of the current intensity is given by

$$\langle \mathbf{N}|\hat{J}_x|0\rangle = (-1)^{\alpha+N_{\mathrm{F}}}\langle \beta|\hat{v}_x|\alpha\rangle \qquad (46)$$

for the Fock state (44) and zero otherwise. Moreover, we notice that the energy of this Fock state (44) is equal to

$$E_{\mathbf{N}} - E_0 = \epsilon_\beta - \epsilon_\alpha. \qquad (47)$$

The energy of the single-particle state $|\alpha\rangle$ is below the Fermi energy $\epsilon_\alpha < \epsilon_{\mathrm{F}}$, while the situation is opposite for the state $|\beta\rangle$: $\epsilon_\beta > \epsilon_{\mathrm{F}}$.

Therefore the conductivity (35) can be expressed in terms of single-particle wave functions of the quantum graph as

$$\sigma_{xy} = \frac{1}{iV}\sum_{\epsilon_\alpha < \epsilon_{\mathrm{F}}}\sum_{\epsilon_\beta > \epsilon_{\mathrm{F}}} \frac{\langle \beta|\hat{v}_x|\alpha\rangle\langle \alpha|\hat{v}_y|\beta\rangle - (x \leftrightarrow y)}{(\epsilon_\alpha - \epsilon_\beta)^2}. \qquad (48)$$

B. Quantization of transverse conductivity

We consider the single-particle wave functions (11) and (12) with the periodic boundary conditions (22). The corresponding single-particle Hamiltonian is defined by

$$\hat{H} = \frac{1}{2}(-i\partial_x - A_x + k_x)^2 + \frac{1}{2}(-i\partial_y - A_y + k_y)^2, \quad (49)$$

where k_x and k_y are the components of the wave vector. The latter are Bloch parameters which take their values on the first Brillouin's zone of the reciprocal space: $k_x \in \left[-\frac{\pi}{ql_x}, \frac{\pi}{ql_x}\right]$ and $k_y \in \left[-\frac{\pi}{l_y}, \frac{\pi}{l_y}\right]$. The velocity operator is given in terms of this Hamiltonian by

$$\hat{v}_x = \frac{\partial \hat{H}}{\partial k_x}. \quad (50)$$

We consider the Hamiltonian eigenstates $u_\alpha^{(n,b)}$ which satisfy Schrödinger's equation

$$\hat{H} u_\alpha^{(n,b)} = \epsilon_\alpha u_\alpha^{(n,b)} \quad (51)$$

and the periodic boundary conditions (22). Differentiating the eigenvalue equation (51) with respect to one component of the wave vector and taking the scalar product with another eigenstate, we get

$$\langle \beta | \hat{v}_x | \alpha \rangle = \langle \beta | \frac{\partial \hat{H}}{\partial k_x} | \alpha \rangle = (\epsilon_\alpha - \epsilon_\beta) \langle \beta | \frac{\partial \alpha}{\partial k_x} \rangle \quad (52)$$

with the short notations $|\alpha\rangle \equiv |u_\alpha\rangle$ and $|\partial_{k_x}\alpha\rangle \equiv |\partial_{k_x} u_\alpha\rangle$.

Using the relation $\langle \beta | \partial_{k_x}\alpha \rangle = -\langle \partial_{k_x}\beta | \alpha \rangle$ obtained by differentiating the orthonormality condition $\langle \alpha | \beta \rangle = \delta_{\alpha\beta}$ together with the completeness relation $(\Sigma_{\epsilon_\alpha < \epsilon_F} + \Sigma_{\epsilon_\alpha > \epsilon_F})|\alpha\rangle\langle\alpha| = \hat{I}$, we find that the conductivity can be written as[10]

$$\sigma_{xy} = \frac{1}{iV} \sum_{\epsilon_\alpha < \epsilon_F} \left\langle \frac{\partial \alpha}{\partial k_y} \Big| \frac{\partial \alpha}{\partial k_x} \right\rangle - \left\langle \frac{\partial \alpha}{\partial k_x} \Big| \frac{\partial \alpha}{\partial k_y} \right\rangle. \quad (53)$$

If the Fermi level falls inside a spectral gap, the sum $\Sigma_{\epsilon_\alpha < \epsilon_F}$ over all the states $|\alpha\rangle$ below the Fermi level can be decomposed into a sum over the occupied bands and a sum over the states $|\alpha\rangle$ inside a band. This latter can be performed as an integral over the values of the Bloch parameters in the first Brillouin zone which forms a torus $\mathbb{T}^2$. Accordingly, we have that

$$\sum_{\epsilon_\alpha < \epsilon_F} = \sum_{\text{occ. bands}} \sum_{\epsilon_\alpha \text{ in occ. band}} = \sum_{\text{occ. bands}} \frac{V}{(2\pi)^2} \int_{\mathbb{T}^2} d\mathbf{k}. \quad (54)$$

Finally, using Stokes theorem in order to transform the two-dimensional integral over the torus into a line integral over the border of the torus, the transverse conductivity becomes

$$\sigma_{xy} = \frac{e^2}{2\pi i h} \sum_{\text{occ. bands}} \oint \left(\left\langle \alpha \Big| \frac{\partial \alpha}{\partial k_x} \right\rangle dk_x + \left\langle \alpha \Big| \frac{\partial \alpha}{\partial k_y} \right\rangle dk_y \right), \quad (55)$$

where the dimensional factor e^2/h with $h = 2\pi\hbar$ has been reintroduced.[10]

The above expression has a well-known topological interpretation: it is the integration of Berry's curvature $\mathcal{F} = \langle \frac{\partial \alpha}{\partial k_\mu} | \frac{\partial \alpha}{\partial k_\nu} \rangle dk_\mu \wedge dk_\nu$ over the base space $\mathbb{T}^2$ of a principal fiber bundle $F[\mathbb{T}^2, U(1)]$. The number $Ch_1 = \frac{i}{2\pi} \int_{\mathbb{T}^2} \mathcal{F}$ is a topological invariant referred to as *Chern number* and is necessarily an integer. Thouless *et al.* showed that the Hall conductivity (55) is given by $\sigma_{xy} = \frac{e^2}{h} \Sigma_{\epsilon_\alpha < \epsilon_F} (t_r - t_{r-1})$ for Hofstadter's model, where t_r is the solution of a diophantine equation

$$r = qs_r + pt_r, \quad (56)$$

which gives the rth gap's position of the Hofstadter spectrum in terms of the integers p and q of the magnetic flux $\Phi = p/q$. When the Fermi level is exactly situated in the rth gap, one finds that $\sigma_{xy} = t_r e^2/h$. The Chern number t_r being an integer one gets the quantization law observed by von Klitzing.[9]

Now, we show that this result extends to quantum graphs. We suppose that the wave functions accumulate the phase $u_\alpha \sim \exp(i\theta_\alpha)$ along the border $\partial\mathbb{T}^2$ of the torus where the line integral of Eq. (55) is carried out, in which case one can write Eq. (55) in the following way:

$$\sigma_{xy} = \frac{e^2}{2\pi h} \sum_{\text{occ. bands}} \oint_{\partial\mathbb{T}^2} \left(\frac{\partial \theta_\alpha}{\partial k_x} dk_x + \frac{\partial \theta_\alpha}{\partial k_y} dk_y \right). \quad (57)$$

In the weak-coupling limit $r \to 0$, the anisotropy parameter (17) is large and the generalized Harper equation (19) reduces to the approximate eigenvalue equation

$$\cos kl_y \simeq \cos(2\pi\Phi n - k_y l_y) \quad (58)$$

with $n \in \mathbb{Z}$. These equations form crossing curves in the plane of the wave number k versus the Bloch parameter k_y. The crossings are exact if $r = 0$, but avoided crossings exist if r is small but nonvanishing. In this case, it is possible to calculate the phase θ_α accumulated by the eigenstate u_α at each avoided crossing, in a way similar to the one shown for tight-binding models by Kohmoto.[17] We obtain that the eigenstates $u_{k_x k_y}$ undergo the transformation

$$u_{k_x k_y} \to u_{k_x k_y}[-e^{iqk_x l_x(t_r - t_{r-1})}] \quad (59)$$

when a loop is performed around the first Brillouin zone. One eventually finds that the Hall conductance is given by

$$\sigma_{xy} = \frac{e^2}{2\pi h} \sum_{\epsilon_\alpha < \epsilon_F} \underbrace{\int_{-\pi/ql_x}^{\pi/ql_x} dk_x \frac{\partial \theta}{\partial k_x}}_{2\pi(t_r - t_{r-1})}$$

$$= \frac{e^2}{h} \sum_{\epsilon_\alpha < \epsilon_F} (t_r - t_{r-1})$$

$$= \frac{e^2}{h} t_r, \quad (60)$$

where we have supposed the Fermi level ϵ_F in the rth gap.

C. Phase diagrams of transverse conductivity

The phase diagram which describes the integer quantum Hall effect for Hofstadter's model has been introduced by
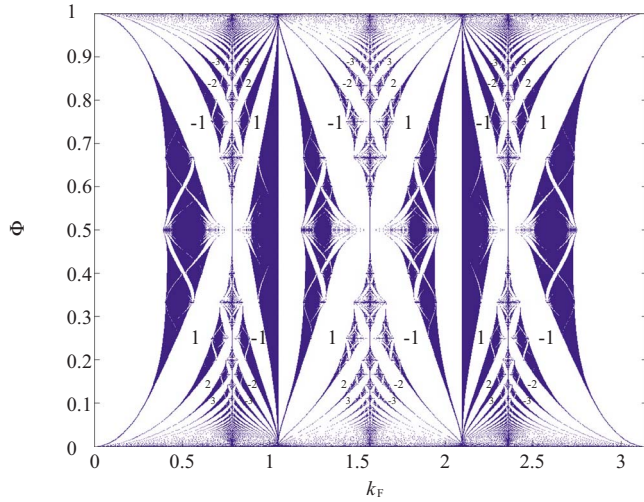
FIG. 8. (Color online) Spectrum and phase diagram for a 2D quantum graph characterized by $l_x=3$, $l_y=1$, and $r=1$. The horizontal axis is the Fermi wave number $k_F=\sqrt{2\epsilon_F}$ and the vertical axis the magnetic flux Φ. The different phases correspond to the integer values of the Hall conductivity computed inside the gaps. As in the situation depicted in Fig. 3(c) we have $l_x=n$ and $l_y=1$, with $n=3$, and we find exactly $n=3$ butterflylike structures for $k \in [0, \pi]$.

Osadchy and Avron.[11] This diagram shows in a beautiful fractal structure the value of the Hall conductivity as a function of the magnetic flux and the Fermi energy of the system. Such a phase diagram can be drawn for quantum graphs as well. The result is straightforward for the *self-dual* case $l_x=l_y$,[18,22] for which the diagram is a nonlinear deformation of the one obtained by Osadchy and Avron.[11] In order to get the phase diagram of an arbitrary graph, we have solved numerically the generalized Harper equation and resolved the diophantine equation (56) for each gap of the spectrum. The phase diagram for the case $l_x=3$ and $l_y=1$ is drawn in Fig. 8 as a function of the Fermi wave number $k_F=\sqrt{2\epsilon_F}$ and the magnetic flux Φ. The quantum phases correspond to the different integer values of the Hall conductivity computed inside the gaps.

A phase diagram describing the IQHE is also obtained for the three-dimensional system described in Sec. III. The Chern numbers evaluated inside the numerous gaps of the initial butterfly ($\gamma=0$) are maintained while the spectrum undergoes the transformation $\gamma \rightarrow 1$. We draw the phase diagram corresponding to the 3D quantum graph in Fig. 9.

V. CONCLUSION

In this paper an important aspect of the quantum transport on 2D and 3D graphs has been studied, namely the quantization of the system's Hall conductivity. First, we have obtained the energy spectra of quantum graphs without and with magnetic field. We showed that their eigenvalue equation can be mapped onto a generalized Harper equation in the case of a 2D rectangular lattice. A 3D rectangular lattice has also been considered.

In zero magnetic field, the graphs have continuous band spectra because of their spatial periodicity and the spectra are
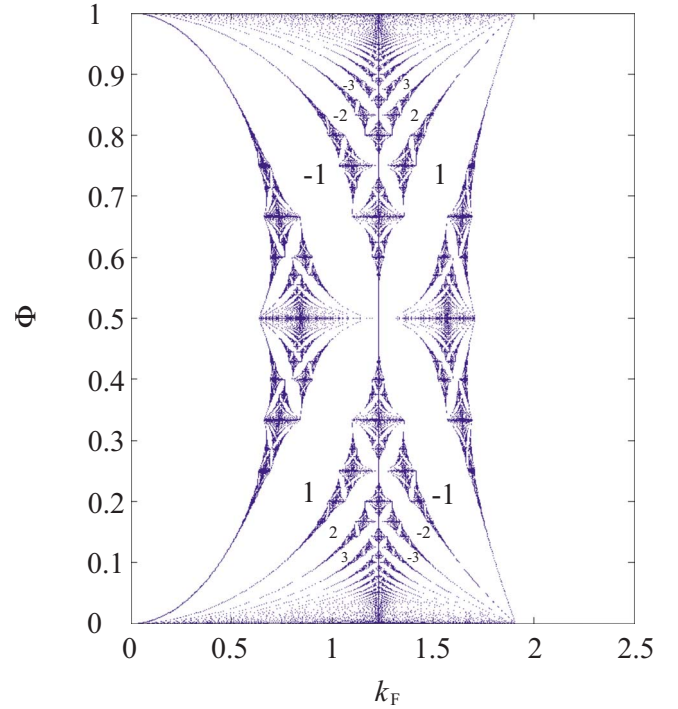

FIG. 9. (Color online) Spectrum and phase diagram for a 3D quantum graph characterized by $l_x=l_y=l_z=1$. The horizontal axis is the Fermi wave number $k_F=\sqrt{2\epsilon_F}$ and the vertical axis the magnetic flux Φ. The different phases correspond to the integer values of the Hall conductivity computed inside the gaps.

discrete at fixed values of Bloch's parameters. The 2D and 3D graphs are shown to differ by their level spacing statistics. Indeed, the 2D graph has at most two incommensurate bond lengths so that its level spacing distribution typically presents a gap around zero spacing. In contrast, the 3D graph has at most three incommensurate bond lengths which is sufficient for Wigner repulsion to manifest itself in the level spacing statistics. On the other hand, both the 2D and 3D graphs are classically chaotic with a positive Kolmogorov-Sinai entropy per unit time in the classical limit.

In nonzero magnetic field, we have obtained fractal energy spectra. A deformed version of Hofstadter's butterfly is recovered in the case of a 2D lattice with the C_4 square symmetry. If the lattice becomes anisotropic, some gaps are filled and the corresponding zones darken in the spectrum due to the appearance of continuous parts in the spectrum. Nevertheless, other gaps remain which are characterized by Chern's topological quantum numbers. We show that the transverse conductivity is quantized in terms of Chern's numbers, as in the integer quantum Hall effect. We construct the fractal quantum phase diagrams of the transverse conductivity.

In conclusion, quantum graphs show rich structures such as fractal spectra and reveal interesting quantum properties such as those emphasized in this work. These versatile models are promising for the exploration of quantum phenomena in condensed matter systems such as the quantum Hall effects.

[1] S. Alexander, Phys. Rev. B **27**, 1541 (1983).

[2] S. Alexander, Phys. Rev. B **29**, 5504 (1984).

[3] J. Avron, A. Raveh, and B. Zur, Rev. Mod. Phys. **60**, 873 (1988).

[4] L. Pauling, J. Chem. Phys. **4**, 673 (1936).

[5] T. Kottos and U. Smilansky, Phys. Rev. Lett. **79**, 4794 (1997).

[6] F. Barra and P. Gaspard, J. Stat. Phys. **101**, 283 (2000).

[7] F. Barra and P. Gaspard, Phys. Rev. E **65**, 016205 (2001).

[8] F. Barra and P. Gaspard, Phys. Rev. E **63**, 066215 (2001).

[9] K. von Klitzing, Rev. Mod. Phys. **58**, 519 (1986).

[10] D. J. Thouless, M. Kohmoto, M. P. Nightingale, and M. den Nijs, Phys. Rev. Lett. **49**, 405 (1982).

[11] D. Osadchy and J. Avron, J. Math. Phys. **42**, 5665 (2001).

[12] D. R. Hofstadter, Phys. Rev. B **14**, 2239 (1976).

[13] N. Goldman and P. Gaspard, Europhys. Lett. **78**, 60001 (2007).

[14] G. Petschel and T. Geisel, Phys. Rev. Lett. **71**, 239 (1993).

[15] D. Springsguth, R. Ketzmerick, and T. Geisel, Phys. Rev. B **56**, 2036 (1997).

[16] P. Exner and R. Gawlista, Phys. Rev. B **53**, 7275 (1996).

[17] M. Kohmoto, Phys. Rev. B **39**, 11943 (1989).

[18] Y. Hasegawa, Y. Hatsugai, M. Kohmoto, and G. Montambaux, Phys. Rev. B **41**, 9174 (1990).

[19] M. Koshino, H. Aoki, K. Kuroki, S. Kagoshima, and T. Osada, Physica B **298**, 97 (2001).

[20] M. Koshino, H. Aoki, K. Kuroki, S. Kagoshima, and T. Osada, Phys. Rev. Lett. **86**, 1062 (2001).

[21] M. Koshino, H. Aoki, T. Osada, K. Kuroki, and S. Kagoshima, Phys. Rev. B **65**, 045310 (2002).

[22] S. Aubry and G. André, Ann. Isr. Phys. Soc. **3**, 133 (1980).